ARMA 22–280

Comparison of Measured and Modeled Casing Deformations of a Test Well in a Longwall Abutment Pillar

Peter Zhang and Daniel Su
NIOSH, Office of Mine Safety and Health Research, Pittsburgh, Pennsylvania, USA
Bo Hyun Kim
NIOSH, Spokane Mining Research Division, Spokane, Washington, USA
Evan Midler
Alliance Coal, LLC, Valley Grove, West Virginia, USA

ABSTRACT: Shale gas wells in longwall abutment pillars are subjected to longwall-induced ground movements, and their stability has been a safety concern for both the mining and gas industries. To understand the impact of longwall mining on the stability of gas wells in longwall abutment pillars, a test well was drilled in a longwall pillar between two adjacent longwall panels to measure longwall-induced deformations in the casing as the two longwall panels on either side were retreated. The longwall panels extracted the Pittsburgh coal seam under a depth of 177 m and were developed with a 3-entry system with 52-m-wide chain pillars and 366-m-wide panels. Casing deformations induced by longwall mining were measured by 60-arm caliper logging and observed with a downhole camera. A FLAC3D model was set up to predict longwall-induced stresses and deformations in the test well casing. The model was validated with measured surface subsidence and longwall-induced pillar pressure. Both measurements and numerical modeling showed that the casing deformed because of relative displacements along distinct weak rock interfaces. Casing deformations at the weak claystone interfaces were found to be confined within the claystone layers. In this case, casing deformations occurred at the same locations with both first and second panel mining. Second panel mining caused additional deformations as the relative horizontal displacements along the interfaces shifted in the opposite direction. The FLAC3D model proved to be capable of predicting the locations and magnitudes of casing deformations with reasonable accuracy.

1. INTRODUCTION

When gas wells penetrate through coal seams in the vicinity of longwall gob, they are subjected to longwall-induced subsurface movements, and casing deformations could occur at certain locations. Longwall-induced deformations in the casing could diminish casing integrity and allow high pressure gas to leak into the mine, potentially causing fires or explosions. Over the past decade, over 1,500 shale gas wells have been drilled in the coal reserves of the Pittsburgh coal seam. The influence of longwall mining on these shale gas wells will have to be evaluated as future longwall panels are mined. Therefore, it is important to understand how longwall-induced subsurface movements and stresses affect gas well casings and to develop engineering guidelines to safely mine-by these shale gas wells.

Longwall-induced subsurface movements and casing deformations have been studied by Su (2016, 2017), Su et al. (2018, 2019), Scovazzo (2018), Zhang et al. (2019), and Zhang and Su (2021). Using instrumentation and numerical modeling techniques, these studies have greatly helped to understand overburden movements and casing deformations over longwall pillars. The first comprehensive instrumentation study conducted in 2013 and 2014 by CONSOL Energy, the Marcellus Shale Coalition, and the Pennsylvania Coal Association evaluated the effect of subsurface strata deformations on the gas well casings above the mining horizon by monitoring the response of test wells in the longwall abutment pillar. The study site was selected over the chain pillars between two 457-m wide longwall panels in a Pittsburgh coal seam longwall mine under 184 m depth of cover. The detailed descriptions of the study site and data analysis were presented by Su (2016 and 2017) and Scovazzo (2018). Su led the field instrumentation and the measurements of casing deformations on four test wells using 60-arm caliper survey after completion of each longwall panel. The caliper surveys showed that the maximum horizontal displacement in all four test wells occurred at a depth of around 119 m at the same location (Su, 2017). Scovazzo (2018) summarized the key findings from this instrumentation study which include: (1) casing deformation was identified in two settings: at the weak/strong rock contacts and within the Pittsburgh Coal Seam; (2) casing deformation was in response to ground movement occurring at weak/strong rock contacts and was above the well intersection with the angle of draw; (3) the most significant movement was found at the weak/strong rock contact on top of Limestone D with horizontal movements in all of the four test wells from 5.1 cm to 14.0 cm.

Zhang and Su (2021) modeled the comprehensively instrumented gas well study case using FLAC3D to further investigate how geological factors influence the stability of shale gas wells in longwall chain pillars under shallow cover. The modeling study found that horizontal movements over longwall chain pillars are also affected by coal seam and overburden dip as well as friction coefficient along the interface. With a one degree of dip away from chain pillars, about one centimeter of additional maximum horizontal displacement could be induced along the gas well. High horizontal movement can occur when claystone interfaces are wet and the frictional coefficient is low. The frictional coefficient at the interface along a saturated claystone layer was found to be as low as 0.05 when a comparison was made between the predicted and measured horizontal movements along the test well casings.

Another instrumentation study was conducted by Su et al., (2019) on gas wells in longwall chain pillars under shallow cover. The study site was located over a southwestern Pennsylvania coal mine employing 457-m-wide longwall panels to extract coal from the Pittsburgh seam under 147-m depth. The longwall panels were developed by a three-entry longwall gate-road system of 18-m × 38-m centers. The study confirmed that under shallow cover, especially under the influence of a major stream valley, longwall-induced subsurface deformations are much higher than those detected under deep cover.

To further understand how shale gas wells in longwall chain pillars are affected by longwall-induced ground movements, a recent study as discussed in this paper was conducted by the coal and gas industry and NIOSH researchers on a test well in the chain pillars between two adjacent longwall panels under an overburden depth of 177 m. 60-arm caliper surveys were performed on the test well casing to measure the longwall-induced deformations after first and second panel mining. A measurement was also made on a longwall-induced pillar pressure increase near the test well. FLAC3D modeling was performed to predict longwall-induced deformations in gas well casings based on site-specific mining and geological conditions. The measurements and modeling results were analyzed and compared to understand longwall-induced casing deformations under shallow cover.

2. TEST SITE DESCRIPTION

The study site discussed in this report was located over the chain pillars between two longwall panels in a West Virginia mine extracting coal from the Pittsburgh seam. Figure 1 shows the panel layout and test well location. A three-entry longwall gate-road system of 15-m × 32-m centers was employed at the mine. The longwall panels were 371-m wide, and the average mining height was approximately 2.1 m. The overburden depth at the test site was 186 m. Figure 1 also shows the location of the test well and underground instrumentation layout. The test well was drilled around the center of the abutment pillar of 27 m rib-to-rib, and the closest distance was 29 m from the test well to the first panel gob and 13 m to the second panel gob. The test well was drilled with a 31-cm hole to a depth of 207 m, about 30 m below the Pittsburgh seam. One 24-cm, J55 casing was installed in the hole to monitor casing deformations as the longwall panel on either side mined by the test site. The thickness of the test well casing was 1 cm. Four borehole pressure cells (BPCs) 6 m apart were placed 8 m horizontally into the abutment pillar for measuring the abutment pillar pressure near the test well. The test site was passed first by first panel mining in August 2020 and then by second panel mining in March 2021. The test well casing was surveyed with a multi-finger caliper and a downhole video camera after each panel mined-by the test site for about 300 m.

The surface contour lines around the test site are also shown in Figure 1. The surface around the test well is not flat but dips down about 30 m to the south and up about 23 m to the north. A creek is present about 150 m on the southeast side of the test well site. Based on the coal seam elevations at the track entry, the coal seam has a dip of about 0.5 degree to the southeast. As surface topography and coal seam dip influence surface and subsurface ground movements, they are considered in the numerical model.

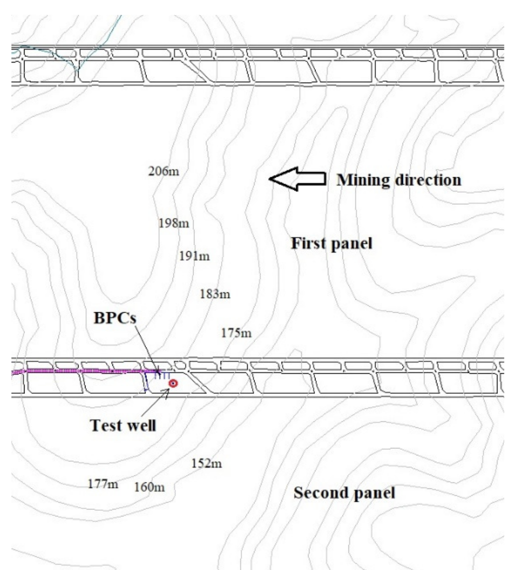

Fig.1. Longwall panel layout and test well location.

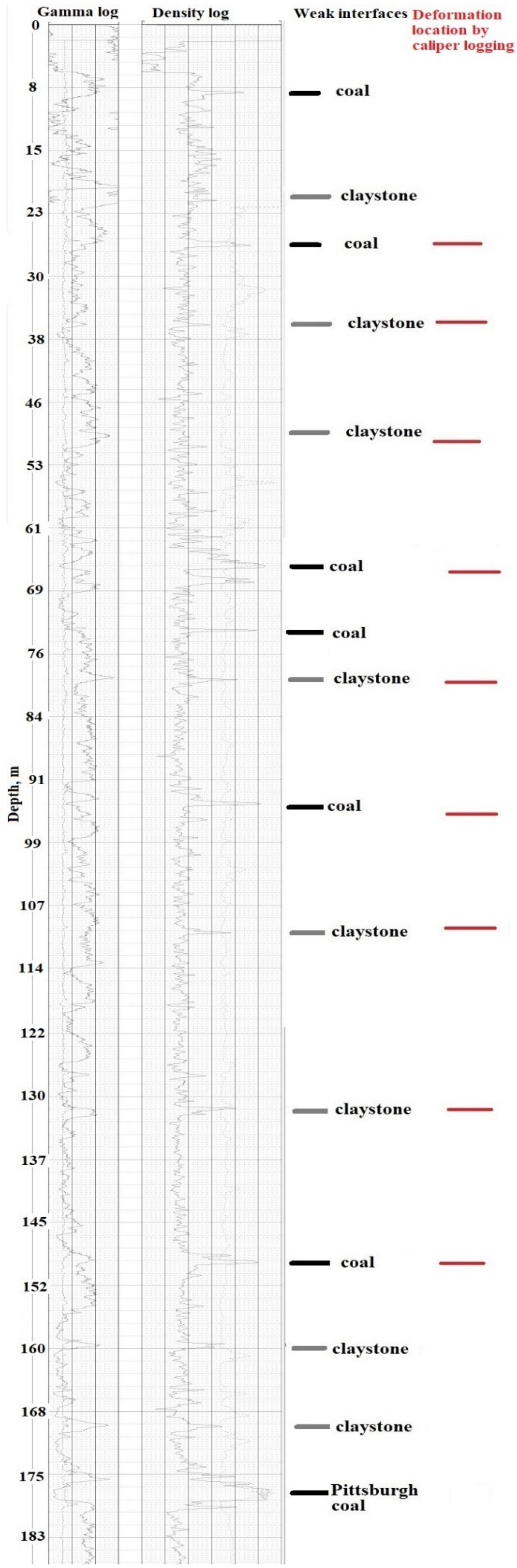

Fig. 2. Test site overburden geology and weak interface locations interpreted by correlating on-site gamma logs and a nearby core hole.

Figure 2 shows the test site overburden geology and interface locations interpreted by correlating an onsite gamma log and a nearby core hole. The overburden geology over the test site is a typical Pittsburgh seam geology and is highlighted by many strong and weak rock interfaces along weak layers like claystone and coal. The claystone and coal interfaces are identified from the gamma log and density log. The weak interfaces represent the weak bedding between a weak layer and a relatively strong massive strata and are implemented in the FLAC3D model.

3. NUMERICAL MODEL AND VERIFICATION

Numerical modeling provides an effective tool for quantitatively assessing the influence of longwall mining on gas wells in longwall pillars. NIOSH researchers have developed FLAC3D modeling techniques to calculate longwall-induced stresses and deformations (Zhang and Su, 2021; Su et al., 2018, 2019; Zhang et al., 2019; and Tulu et al., 2017). In this study, the FLAC3D model (Itasca, 2017) was set up based on the geological conditions and longwall mining layouts around the test well site. Figure 3 shows the cross-sectional view of the FLAC3D model. The model included overburden from the Pittsburgh seam all the way up to the surface. The overburden lithology was based on the lithology from the nearest core hole around the test well site. Table 1 shows the rock properties used in the model. The weak bedding interface locations were based on the on-site gamma logs. Surface slope over the longwall panel was also modeled. The longwall caving zone was modeled by strain-hardening material implemented by the "FISH" scripting language in FLAC3D (Itasca, 2017). The overburden strata above the caving zone were modeled with ubiquitous joint material, and the coal seam, immediate roof, and floor were modeled with Mohr-Coulomb materials. In-situ horizontal stresses were applied in the model with the maximum horizontal stress of three times the vertical stress along the panel and the minimum horizontal stress of two times the vertical stress across the panel. The test well casing and cement filling were modeled according to their mechanical properties as shown in table 2. The steel casings were modeled with von Mises material, and the cement fillings were modeled with Mohr-Coulomb material. The casing was installed in the model before the longwall gate entries were developed.

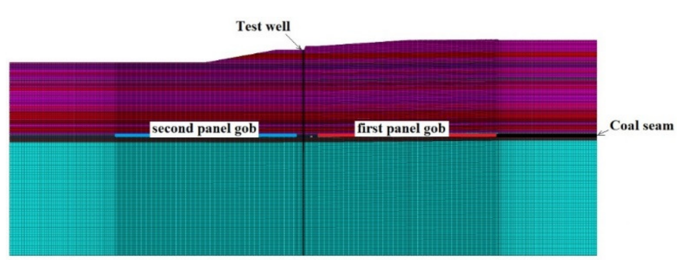

Fig. 3. Sectional view of the FLAC3D model.

Table 1. Rock properties used in the model

Rock Type	Young's Modulus, Mpa	Poisson's Ratio	Cohesion, Mpa	Internal Friction Angle, degrees	Tensional Strength, Mpa
coal	2,070	0.30	1.9	28	0.3
claystone	2,900	0.3	1.9	28	0.3
shale	11,600	0.25	11.7	35	4.5
sandyshale	11,600	0.25	11.7	35	4.5
sandstone	11,600	0.25	17.9	35	6.9
limestone	17,400	0.22	15.9	35	6.1
shaley limestone	17,400	0.22	14.5	38	5.9
shaley sandstone	15,000	0.22	11.7	38	4.8
siltyshale	11,600	0.25	11.7	32	4.2

Table 2. Input parameters for test well casing and cement filling in the model

Test well component	Outside Diameter, cm	Wall Thickness, cm	Young's Modulus, MPa	Poisson's Ratio	Yield Strength, MPa
Test casing	24.4	1.0	2.0×10^5	0.3	345.0
Cement filling	31.0	6.5	6.9×10^3	0.25	13.8

The FLAC3D model for the study site is set up based on site-specific mining and geologic conditions, and surface subsidence and pillar pressure are used to verify the model. Figure 4 shows predicted final surface subsidence across the test well and the longwall panels after each of the panels is completed. The predicted final subsidence curve is almost flat around the panel center but is asymmetrical due to the presence of surface slope above the panel. The model predicts a maximum subsidence of about 1.31–1.34 m around the panel center. At the gas well location, the predicted surface subsidence is about 3.0 cm after first panel mining and 9.7 cm after second panel mining. The subsidence is small at the test well site because the overburden is shallow. Surface subsidence was measured at the test well site after first panel mining, and it was almost zero. Based on the experience of surface subsidence in Pittsburgh seam longwalls, the predicted surface subsidence is accurate in terms of subsidence profile and maximum subsidence factor.

Figure 5 shows the predicted vertical stress distribution across the chain pillars at the coal seam horizon after first and second panel mining. At the coal seam horizon, the gas well is mainly influenced by the longwall-induced vertical stress in the coal pillar near the well. The predicted pillar pressure increase at the test well location is about 2 MPa after first panel mining and 4 MPa after second panel mining. A longwall-induced pillar pressure increase near the test well was measured by borehole pressure cells (BPCs) as the first panel mined-by the test site, and the measured pillar pressure increase is shown in Figure 6. The BPCs were installed horizontally 8.2 m into the abutment pillar from the track entry. The measured pillar pressure increase was 4.1 MPa after first panel mining. The predicted pillar pressure increase at the BPC location was 4.3 MPa after first panel mining. By comparison, the model reasonably predicts the longwall-induced vertical stress around the chain pillars.

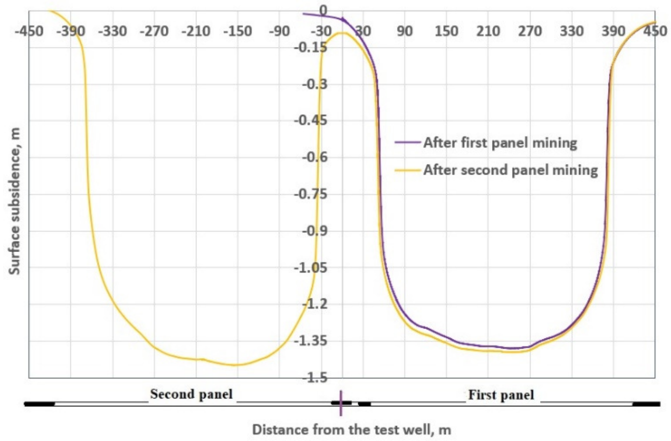

Fig. 4. Predicted final surface subsidence across the chain pillars and two longwall panels after first and second panel mining.

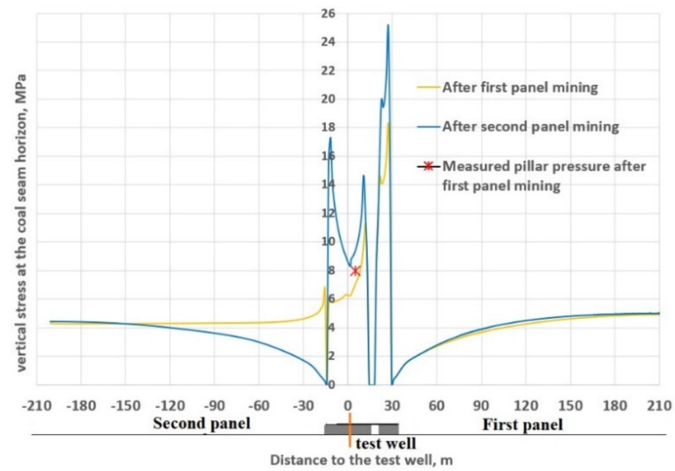

Fig. 5. Predicted vertical stress distribution at the coal seam horizon and measured pillar pressure near the test well.

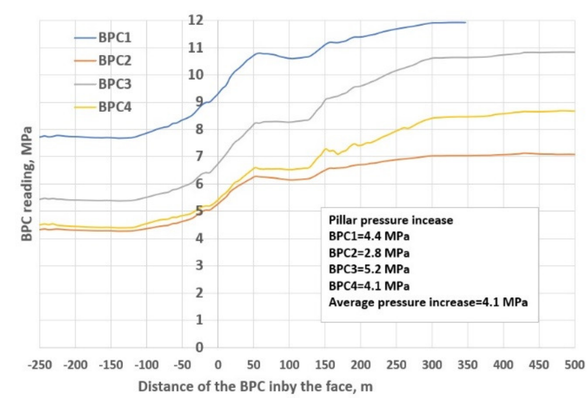

Fig. 6. Measured pillar pressure increase using BPCs with first panel mining.

4. COMPARISON OF PREDICTED AND MEASURED CASING DEFORMATIONS

The model predicted horizontal displacement along the test well casing after first panel mining as shown in Figure 7. After first panel mining, the casing moves towards the first panel gob. At the surface, the casing moves about 2 cm towards the gob. In the subsurface, the casing is also subjected to relative horizontal displacements or shear displacements at interface locations. Casing deformations are caused by relative horizontal displacements along strong/weak rock interfaces. Based on the horizontal displacement curve, the casing deformations are predicted at the locations shown in Figure 7. With second panel mining, the casing moves towards the second panel gob. Figure 8 shows the predicted horizontal displacement along the test well casing after second panel mining. The displacement curve indicates that casing deformations occur at the same locations after second panel mining.

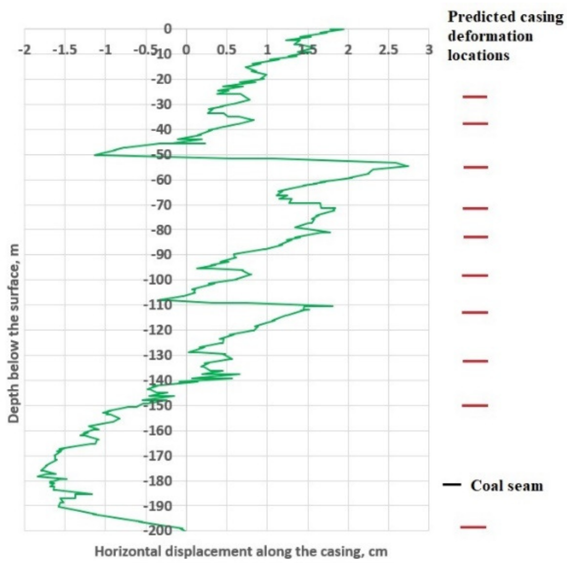

Fig. 7. Predicted horizontal displacement and deformation locations along the test well casing after first panel mining.

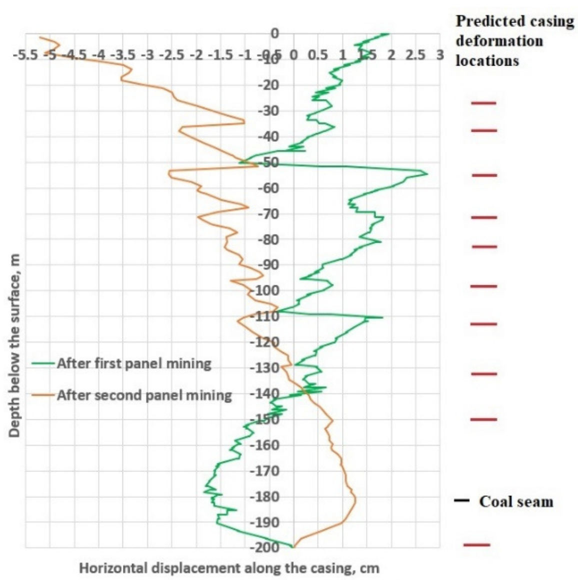

Fig. 8. Predicted horizontal displacement and deformation locations along the test well casing after second panel mining.

The casing deformations were measured by 60-arm caliper logging after first and second panel mining. Figure 9 shows the measured casing inside diameter changes after first panel mining. The nominal casing inside diameter for the 9-5/8-in casing is 22.4 cm. This figure shows that the casing diameters reduced when the casing deformed. Casing deformations were detected at 10 locations below the surface. The largest diameter reduction was 6.8 cm at 51 m below the surface, and the diameter reduction at other locations was less than 1 cm.

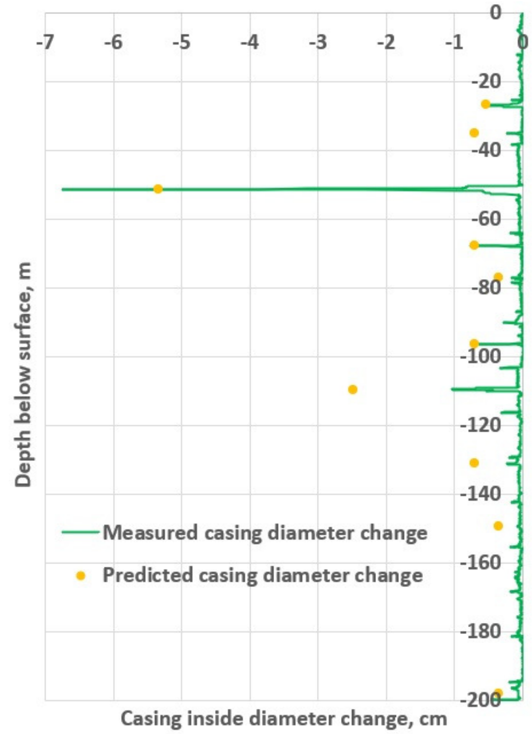

Fig. 9. Measured and predicted casing minimum inside diameter changes after first panel mining.

The measured and predicted casing diameter changes after first panel mining are summarized in Table 3. The minimum casing diameter change is estimated from the predicted relative displacement multiplied by a factor of 1.4. This factor is determined by analyzing the caliper-logging data. From the caliper survey, the casing becomes ovalized after being deformed. The deformed casing along the minimum diameter tends to be oriented perpendicular to the longwall mining direction. A diameter increase along the mining direction is also measured by caliper logging, but the casing minimum diameter change is used for analyzing casing deformation because the diameter reduction across the panel is the result of shear displacement. Under the shear displacement at an interface across the longwall mining direction, the casing deforms on two sides opposite to each other. One side is the active side subjected to active force, and the other side is the reactive side. The deformation on the active side generally represents the relative horizontal displacement along the interface. Based on the results of the caliper survey on the test well, the deformation at the reactive side is about 40% of the amount at the active side. The deformation at each side causes a radius change in the casing. The sum of the radius changes is the casing minimum diameter change to be estimated at about 1.4 times the predicted horizontal relative displacement. For comparison, the predicted casing diameter changes are also plotted in Figure 9, which shows that the prediction and measurement are in reasonable agreement in both locations and magnitudes.

Table 3. Comparison between predicted and measured casing deformations after first panel mining.

Depth below surface, m	Predicted relative displacement, cm	Predicted casing diameter change, cm	Measured casing diameter change, cm
27	0.38	0.53	0.48
35	0.51	0.71	0.20
51	3.81	5.33	6.80
68	0.51	0.71	0.74
77	0.25	0.36	0.18
96	0.51	0.71	0.64
110	1.78	2.49	1.02
131	0.51	0.71	0.20
149	0.25	0.36	0.08
200	0.25	0.36	0.46

Figure 10 shows the measured casing minimum diameter changes after second panel mining. The measured and predicted casing diameter changes after second panel mining are summarized in Table 4. As overburden moves towards the second panel, additional relative horizontal displacement occurs at the same interfaces but in the opposite direction. The total casing diameter change is accumulative. The measurements show that the casing deformations remain at the same locations. The maximum diameter reduction is still at the horizon 51 m below the surface, but the magnitude increases from 6.8 cm to 8.2 cm. The second largest diameter reduction is 3.2 cm which occurs at 110 m below the surface. The casing diameter reductions at other locations increase slightly after second panel mining. The predicted casing diameter changes after second panel mining are also plotted in Figure 10, and by comparison, the prediction reasonably agrees with the measurement. The casing deformation locations are compared with the overburden geology at the test well site as shown in Figure 2. The comparison indicates that all the casing deformations occurred at the weak claystone and coal interfaces.

Table 4. Comparison between predicted and measured casing deformations after second panel mining.

Depth below surface, m	Predicted relative displacement after second panel mining, cm	Predicted accumulative relative displacement, cm	Predicted casing diameter change, cm	Measured casing diameter change, cm
27	0.25	0.64	0.89	0.81
35	1.02	1.52	2.13	0.36
51	1.78	5.59	7.82	8.20
68	0.51	1.02	1.42	1.71
77	0.05	0.30	0.43	0.18
96	0.51	1.02	1.42	1.62
110	1.02	2.79	3.91	3.20
131	0.25	0.76	1.07	0.46
149	0.13	0.38	0.53	0.10
200	0.25	0.51	0.71	0.82

Figure 11 shows a visual view of predicted deformation locations and caliper-detected deformation locations. The predicted deformation locations are generally in good agreement with the measured deformation locations.

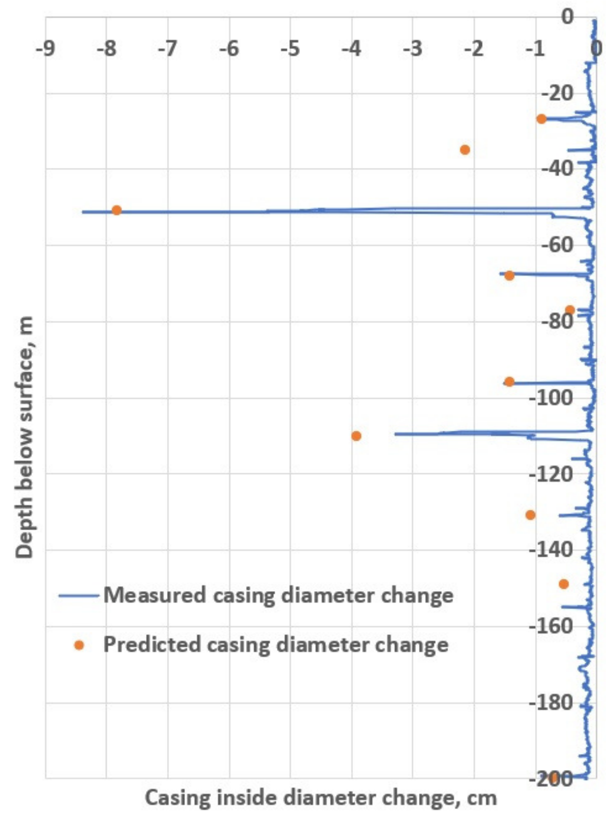

Fig. 10. Measured and predicted casing minimum inside diameter changes after second panel mining.

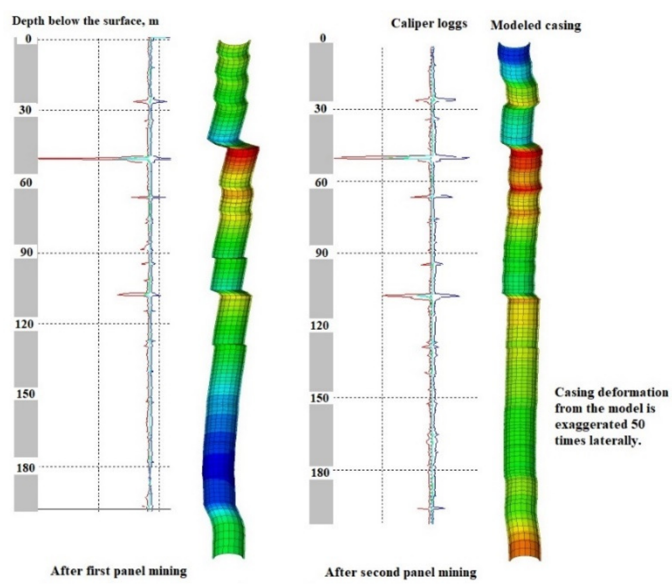

Fig. 11. Comparison of modeled and caliper-surveyed casing deformations.

The test well casing was also surveyed with a downhole video camera after the first panel was mined. Casing deformations were observed at two locations: 51 m and 110 m below the surface. Figure 12 shows the casing deformation observed with the downhole camera at 51 m below the surface where a 6.8-cm casing diameter reduction was detected by the 60-arm caliper logging. At this location, the casing is bulged with shear deformation. The second part of this figure also shows that the deformation location happened to be at a coupler. The debris resting on the top edge of the lower casing suggests that the edge of the casing was kinked in after becoming deformed. Since the casing was connected by joints at the coupler, additional casing deformation could be induced at the coupler with the effect of kinking at the casing edge. Figure 13 shows the casing deformation observed with the downhole camera at 110 m below the surface where about a 1-cm casing diameter reduction was detected by the 60-arm caliper logging after first panel mining. An ovalized shape and a small amount of shearing can be seen from the captured image at the deformation location.

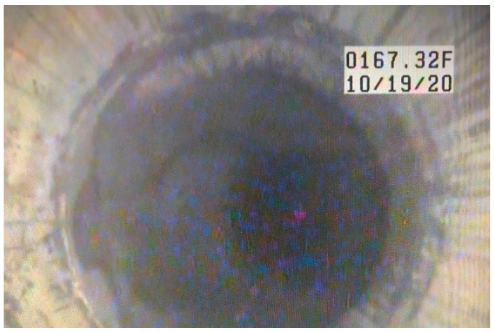

a. Top-down view of the deformation location from the 51-m depth.

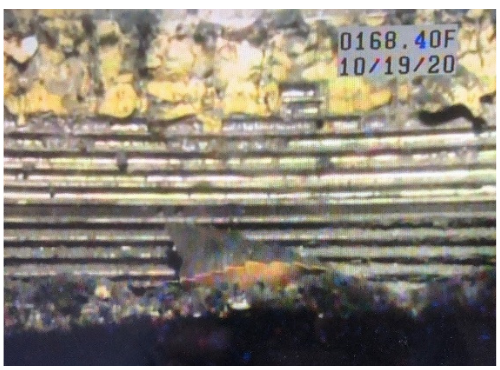

b. Lateral view of the casing wall with coupler joint exposed.

Fig. 12. Casing deformation at 51-m depth viewed with downhole camera.

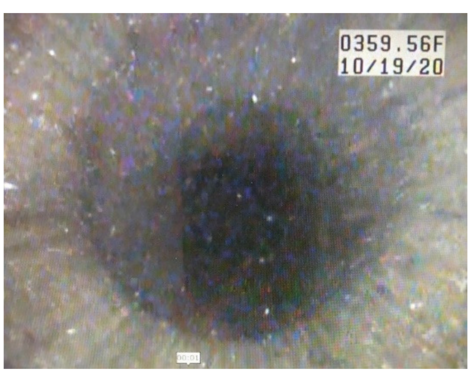

Fig. 13. Casing deformation at 110-m depth viewed with downhole camera.

Stresses in the casing induced by ground movements include three components: vertical, horizontal, and shear. The combination of all the stress components can be represented by von Mises stress. The von Mises stress gives an indication of the casing's stress level compared to its strength capacity and can be used to predict casing yielding. Figure 14 shows the von Mises stress and yielding locations in the intermediate casing. This figure shows that casing deformations occur at locations with high von Mises stress. Above the coal seam, von Mises stress exceeds the casing strength at four locations at the weak interfaces. At the coal seam horizon, the von Mises stress reaches the casing strength after second panel mining because of the higher abutment pressure in the chain pillars.

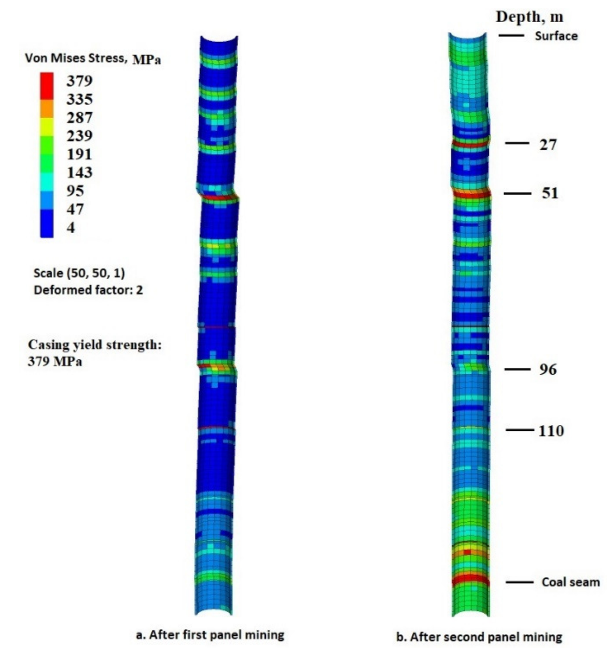

Fig.14. Von Mises stress in the test well casing after first and second panel mining.

5. DEVELOPMENT OF CASING DEFORMATIONS AT THE INTERFACE

At the weak rock interface, casing deformations are induced by the relative horizontal displacement or shear displacement along the interface, and this displacement can be captured by the multi-finger caliper logging. The results of the 60-arm caliper logging in this study have shown that the casing deformation initiates at the bottom of the claystone layer after first panel mining and then propagates upward towards the top of the claystone after second panel mining. The amount and the extent of the deformation depend on the amount of relative horizontal displacement along the interface. By caliper logging, the casing deformation at the interface is confined within the thickness of the weak layer. Figure 15 shows the casing deformations at a 51-m depth after first and second panel mining. The images are rendered from the caliper logging data. According to the core log and gamma logs, the deformations occurred at a 0.9-m claystone layer underlain by a massive limestone layer. After first panel mining, the casing deformations mainly occurred within about 0.3 m of the claystone layer at the bottom. The deformations developed at two opposite sides of the casing is an indication that shear displacement took place along the interface. The white arrows in the Figure 15 indicate shearing directions. The shear displacement is not apparent in the image because the caliper arms were not centralized when passing the interface with a shear displacement. After second panel mining, the deformation propagated upward and extended to the whole claystone layer. As the deformation is induced by shear displacement at the claystone interface, the extent of the deformation is restricted within the claystone layer. The growth of the deformation zones after second panel mining is associated with time-dependent deformation of the claystone and possible claystone weakening due to water saturation.

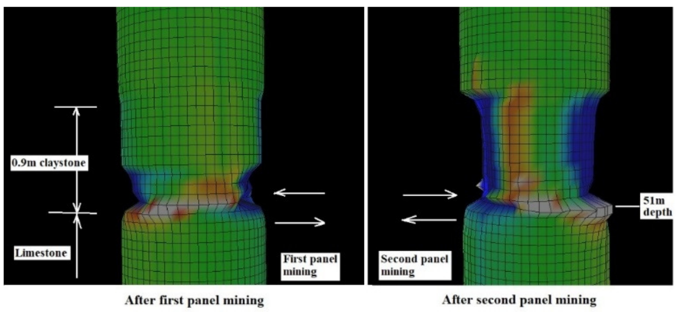

Fig. 15. Development of casing deformation at 51-m depth after first and second panel mining (white arrows indicate shearing directions).

Figure 16 shows the casing deformations at a 0.6-m claystone layer at a 110-m depth after first and second panel mining. This figure shows the deformation develops at a 110-m depth in a similar manner as at a 51-m depth. It clearly indicates that the deformation initiates at the active panel side, at which the deformation is larger. Figure 16 also shows that the extent of the deformation is restricted within the thickness of the claystone layer.

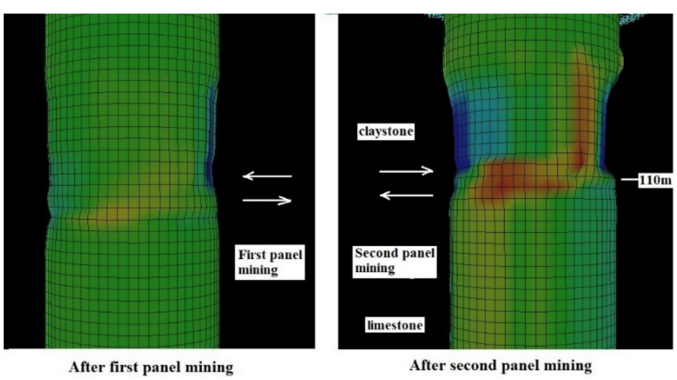

Fig. 16. Development of casing deformation at 110-m depth after first and second panel mining (white arrows indicate shearing directions).

6. CONCLUSIONS

Conclusions and key takeaways derived from comparing field measurement and FLAC3D modeling of casing deformations in a coal/gas operator's test well in a longwall abutment pillar are as follows:

- Casing deformed due to relative displacements along distinct rock interfaces. In this case, casing deformations happened at the same locations for both first and second panel mining.
- Second panel mining caused additional deformations as the relative interface shear displacements shifted in the opposite direction. The largest casing deformation was measured at 51 m below the surface after second panel mining with a total diameter change of 8.2 cm.
- The casing deformation zone at the 51-m depth increased from 0.3 m after first panel mining to 0.9 m after second panel mining due to time-dependent deformation.
- Casing deformations at the distinct strong/weak claystone rock interfaces were confined within the claystone layers.

DISCLAIMER

The findings and conclusions in this report are those of the author(s) and do not necessarily represent the official position of the National Institute for Occupational Safety and Health (NIOSH), Centers for Disease Control and Prevention (CDC). Mention of any company or product does not constitute endorsement by NIOSH.

REFERENCES

ITASCA Consulting Group, Inc. 2017. FLAC3D, Version 6.0, User's Guide.

Scovazzo, V. 2018. Mining effects on gas and oil wells pad NV-35 field experiment field monitoring. In *Proceedings of the 37th International Conference on Ground Control in Mining*. Morgantown, WV: West Virginia University, pp. 30–43.

Su, D.W.H., Zhang, P., Dougherty, H., Van Dyke, M., Minoski, T., Schatzel, S., Gangrade, V., Watkins, E., Addis, J., and Hollerich, C. 2019. Longwall-induced subsurface deformations and permeability changes – Shale gas well casing integrity implication. In *Proceedings of the 38th International Conference on Ground Control in Mining*. Morgantown, WV: West Virginia University, pp. 49–59.

Su, D.W.H., Zhang, P., Van Dyke, M., and Minoski, T. 2018. Effects of longwall-induced subsurface deformations on shale gas well casing stability under deep covers. In *Proceedings of the 37th International Conference on Ground Control in Mining*. Morgantown, WV: West Virginia University, pp. 63–70.

Su, D.W.H. 2017. Effects of longwall-induced subsurface deformations on the mechanical integrity of shale gas wells drilled over a longwall abutment pillar. *2017 SME Annual Meeting*, Feb.19–22, 2017, Denver, CO. Preprint 17-051, pp. 1-6.

Su, D.W.H. 2016. Effects of longwall-induced stress and deformation on the stability and mechanical integrity of shale gas wells drilled through a longwall abutment pillar. In *Proceedings of the 35th International Conference on Ground Control in Mining*. Morgantown, West Virginia, pp. 119–125.

Tulu, I.B., Esterhuizen, G.S., Mohamed, K.M., Klemetti, T.M. 2017. Verification of a calibrated longwall model with field measurements. In *Proceedings of the 51st US Rock Mechanics/Geomechanics Symposium*, 25–28 June 2017. San Francisco.

Zhang, P. and Su, D., 2021. FLAC3D modeling evaluation of the comprehensive NV-35 gas well pillar study. In *Proceedings of the 55th US Rock Mechanics/Geomechanics Symposium*, 20–23 June 2021. Texas.

Zhang, P., Dougherty, H., Su, D., and Trackemas, J. 2019. Influence of longwall mining on the stability of gas wells in chain pillars. In *Proceedings of the 38th International Conference on Ground Control in Mining*, Morgantown, West Virginia, pp. 38–48.